Revision 2

High-pressure aragonite phenocrysts in carbonatite and carbonated syenite xenoliths within an alkali basalt

Vratislav Hurai

Geological Institute, Slovak Academy of Sciences, Dúbravská cesta 9,

840 05 Bratislava, Slovakia

Corresponding author: e-mail: vratislav.hurai@savba.sk

Monika Huraiová

Department of Mineralogy and Petrology, Comenius University,

Mlynská dolina, 842 15 Bratislava, Slovakia

Rastislav Milovský and Jarmila Luptáková

Geological Institute, Slovak Academy of Sciences, Ďumbierska 1,

974 01 Banská Bystrica, Slovakia

Patrik Konečný

State Geological Institute of D. Štúr, Mlynská dolina 1,

817 04 Bratislava, Slovakia

Abstract

We describe the first observation of primary magmatic aragonite in carbonatite and carbonated syenite, occurring as xenoliths in a Pliocene basaltic diatreme located near the Hungary–Slovakia border. The aragonite-hosting matrix consists of disordered P-rich calcite, occasionally associated with trachyte glass. We interpret the aragonite growth as evidence of supra-lithostatic overpressure in the magmatic plumbing system that connected the crustal basaltic reservoir with the partial melting zone of the lithospheric mantle, and the disordered calcite ± trachyte as quenched residual, immiscible melts, generated close to the solidus of the carbonated alkali basalt differentiated in the crustal reservoir. The quenching event was a phreato-magmatic eruption within the stability field of the low-pressure calcite; this was triggered by advective overpressure, caused by expanding gas bubbles in a quasi-incompressible silicate melt system. The high-pressure, pre-eruption origin of aragonite is indicated by enrichment in ^{13}C compared to the associated calcite interpreted as a record of CO_2 degassing at $T > 500$ °C. The oxygen ($\delta^{18}O$ ranges of 22.1–24.5 ‰ V-SMOW in aragonite, 21.6–22.7 ‰ in calcite) and carbon ($\delta^{13}C$ ranges of -4.4 to -5.9 ‰ V-PDB in aragonite, -11.9 to -12.7 ‰ in calcite) isotope signatures are consistent with a degassed carbonatite melt primarily derived from a subduction zone.

Keywords: aragonite, carbonatite**,** syenite, xenolith, alkali basalt, Slovakia

Introduction

Carbonatites are magmatic rocks, whose mantle origin is widely accepted (e.g., Bailey 1993; Harmer and Gittins 1997; Bell and Simonetti 2010). However, the origin of calcic carbonatites remains controversial, because experimental work (e.g., Lee and Willey 1998a, b;

Brooker and Kjarsgaard 2011) has ruled out the generation of $CaCO_3$-dominant liquids devoid of silica and alkalis via magmatic fractionation processes in the crust or the mantle. Consequently, natural calcic carbonatites have been interpreted to represent either degraded alkalic carbonatites modified by sub-solidus alteration and/or loss of alkaline aqueous fluid (Keller and Zaitsev 2006), or as cumulates of calcite crystals that have settled from parental dolomitic carbonatite (Lee and Willey 1998a) or silicate melts (Brooker and Kjarsgaard 2011).

Here we describe aragonite phenocrysts that have crystallized from a calcic carbonatite melt. We document variations in the structural ordering, major element partitioning and isotope composition of calcite and aragonite, thus corroborating the existence of calcic carbonatite liquids in nature. We propose, however, that the magmatic aragonite need not be related to ultra-high-pressure (P > 3 GPa) conditions in the mantle, as proposed by Humpreys et al. (2010), but may reflect episodic supra-lithostatic overpressure in the magmatic plumbing system and the overlying crustal reservoir.

Field evidence, petrography and mineralogy

Carbonatite and carbonated syenite xenoliths with aragonite occur in a diatreme exposed in the center of Hajnáčka village (48°13’5.25’’N, 19°57’18.59’’E, southern Slovakia). The diatreme, towering about 75 m above the surrounding river terrace, represents a feeder conduit of a basaltic maar removed by erosion. The diatreme is composed of palagonitized tuffaceous breccia and scoria breccia, and is intersected by a 2.7 ± 0.5 Ma-old basalt dike (Vass et al. 2007).

The Hajnáčka diatreme is one of numerous monogenetic volcanic centers of the Late Miocene–Late Pleistocene alkali basalt province in the northern part of the intra-Carpathian back-arc basin (Pannonian Basin). The volcanism was triggered by rifting in the orogenic hinterland superimposed on Middle Miocene gravity-driven subduction, which was compensated by diapiric

rise and decompression melting of the asthenosphere (Nemcok et al. 1998; Konečný et al. 2002). The northern Pannonian Basin has been characterized as having high (~80–90 mWm^{-2}) heat flow, moderate (26–28 km) crustal thickness and a 70–90 km-thick lithospheric mantle (Dérerová et al. 2006; Tašárová et al. 2009).

Direct evidence for carbonatitic melts in, and carbonate metasomatism of, the lithospheric mantle beneath Pannonian Basin has been provided by the occurrence of calcite blebs in silicate veins within mantle xenoliths (Chalot-Prat and Arnold 1999; Bali et al. 2002; Demeny et al. 2004, 2010), calcite inclusions and carbonate veins in mafic cumulate xenoliths ejected in Pliocene alkali basalts (Hurai et al. 2007), and carbonatite-bearing mafic cumulate xenoliths in Cretaceous lamprophyre dikes (Guzmicz et al. 2008).

Aragonite-bearing carbonatites described in this study occur as isolated xenoliths and silicate-carbonate fracture infillings in carbonated syenite xenoliths within welded basaltic breccias (Fig. 1a). Two of a total of five carbonatite and carbonated syenite xenoliths contain aragonite and are described in detail in this paper.

The carbonated syenite xenolith HA-8 is composed of potassium feldspar and plagioclase, minor quartz, and accessory ferroan spinel, magnesian ilmenite with inclusions of niobian rutile, hedenbergite replacing aegirine-augite, and apatite enriched in rare-earth elements (REE). The texture of the xenolith resembles those of hydraulic breccias, with angular clasts of quartz, plagioclase, and feldspar cemented by a matrix composed of silicate glass and carbonatitic material. The silicate glass corresponds to a metaluminous alkalic trachyte. In transmitted light, the calcite matrix is polygonal, with a fibrous, radial-concentric microtexture. Aragonite crystals appear freely suspended in the calcite matrix and locally encrust resorbed and fragmented feldspar grains (Fig. 1b).

The carbonatite xenolith HA-9 is composed of bladed aragonite crystal aggregates interlaced with a fibrous polygonal calcite matrix that is texturally identical to that observed in the syenite xenoliths (Fig. 1c). The crystal-to-matrix volumetric ratio was estimated as ~7:3. Apart from the carbonates, no other mineral phases were observed.

The aragonite crystals are essentially pure $CaCO_3$ with 0.69–1.80 wt% SrO (1.17 wt% in average, $N = 14$), low P_2O_5 (0–0.22 wt%, 0.08 wt% in average), and negligible MgO (< 0.05 wt%), whereas the calcite matrix, also dominated by $CaCO_3$, shows increased MgO (1.45–2.93 wt%, 1.9 wt% in average, $N = 8$), P_2O_5 (0.05–0.29 wt%, 0.21 wt% in average), and negligible SrO (< 0.08 wt%) concentrations (Supplementary Table 1). X-ray maps (Fig. 2) corroborate the preferential partitioning of Sr in the aragonite, and Mg and P in the calcite. Slightly increased P in the aragonite overlaps the Sr-rich zones. P and Mg in the calcite behave competitively, creating a feather-like pattern with P concentrated inside fibers and Mg along their periphery. The elemental distribution is consistent with the orientation of fibers seen in polarized transmitted light (Fig. 1c).

Raman spectra of the carbonate crystals and matrix correspond to that of aragonite and calcite I, respectively (Supplementary Fig. 1). The vibration peaks of the calcite are ~3-times broader than those of the associated aragonite and the reference hydrothermal calcite (Supplementary Table 2), being diagnostic of a partly disordered structure.

Raman mapping (Fig. 3) revealed the incremental oscillatory growth zoning of aragonite aggregates, contrasting with an irregular patchy domain texture of the associated calcite matrix. The aragonite growth zoning reflects alternating zones that are Sr-rich and highly fluorescent with zones that are Sr-depleted and moderately fluorescent. The fluorescence is most likely caused by variable Mn and/or REE contents in the Sr-rich zones. In contrast, the patchy texture of

the low-fluorescent calcite matrix is due to variable intensity of the major symmetric stretching $\nu_1 CO_3^{2-}$ band, which reflects uneven structural ordering of individual domains.

The carbonatite HA-9 showed $\delta^{18}O$ values that were approximately constant across the carbonate phases (22.1–24.5 ‰ V-SMOW in aragonite, 21.6–22.7 ‰ V-SMOW in calcite), contrasting with variable $\delta^{13}C$ values (-4.4 to -5.9 ‰ V-PDB in aragonite, -11.9 to -12.7 ‰ in calcite).

Discussion and geologic implications

Contrasting isotope ratios in aragonite and calcite from Hajnáčka rule out a secondary low-temperature hydrothermal alteration/precipitation. In addition, several lines of spectroscopic (patchy domains with $\nu_1 CO_3^{2-}$ bands of variable intensities, vibration bands broadening), textural (polygonal fibrous texture similar to that of rapidly frozen brines), and compositional (increased Mg and P) evidence suggest that the calcite matrix is a quenched carbonatite liquid, which underwent CO_2 degassing at $T > 500$ °C, when the CO_2 gas is isotopically heavier than the associated calcite (Chacko et al. 1991). The greater $\delta^{13}C$ values in aragonite are thus consistent with crystallization from the carbonatite melt prior to degassing.

The *P*-*T* stability limit of aragonite-bearing carbonatite melt is defined by the aragonite-calcite II-carbonatite liquid-aqueous fluid equilibrium curve of the CaO-CO_2-H_2O system (Fig. 4), extending from 580 °C and 1.22 GPa to higher *T* and *P* (Wyllie and Boetcher 1969). The minimum pressure of 1.22 GPa at the aragonite solidus substantially exceeds the lithostatic load of the 26-km-thick crust in the study area, assuming an average crust density of 2,700 $kg.m^{-3}$ (~0.7 GPa), thus favoring crystallization of the aragonite in the mantle. However, the low Mg content in the calcite matrix is out of equilibrium with Mg-rich mantle minerals. Moreover, the

sharp edges and local growth onto resorbed anorthoclase grains fragmented within the calcite matrix rule out the mantle origin of the aragonite, because the absence of corrosion and resorption features is inconsistent with the isothermal decompression in basaltic magma ascending from mantle depths. In addition, preservation of pristine mantle aragonite in magmas residing and fractionating in crustal reservoirs is precluded by the extremely rapid kinetics (few hours) of the aragonite-to-calcite transformation at $T > 600$ °C (Hacker et al. 1992).

One explanation consistent with our observations is that the aragonite crystallized due to dynamic overpressurization of a volatile magma conduit (Sahagian and Proussevitch 1992). According to this concept, a volatile-rich alkali basalts ascending from the partial melting zone at the base of lithospheric mantle may generate short-lived overpressure in the crustal magma reservoir through the interconnected melt network that becomes filled with rising and expanding gas bubbles. The system remains sealed and pressure rises until failure occurs and eruption is triggered. The explosive discharging leads to entrainment of fragmented flotation cumulate with residual melts and aragonite phenocrysts from the top of the fractionated basalt reservoir into incoming pristine basalt, and instantaneous quenching of the metastable aragonite-calcite assemblage in the calcite I stability field at low P and T. An overpressure of at least 0.6 GPa, i.e. ~186% of the local lithostatic load, would be needed to stabilize aragonite instead of calcite phenocrysts close to the solidus of the carbonated alkali basalt that underplated the ~26-km-thick crust (Fig. 4).

The origin of calcic carbonatite is not fully understood. Its association with alkaline silicate igneous complexes (Harmer 1999; Woolley and Kjarsgaard 2008) and rifted regions (Harmer and Gittins 1997) suggests formation by differentiation of a mantle-derived parental melt (Bell and Simonetti 2010), although experimental work (Lee and Willey 1998b, Brooker and Kjarsgaard 2011) has ruled out silicate-carbonate liquid immiscibility, fractionation, or direct

partial melting of a mantle source as the mechanisms capable of generating essentially pure calcic carbonatite liquid at any *P-T*. However, alkali- and Mg-poor calcic carbonatites are generated in subduction zones by partial melting of carbonated metapelite (Thomsen and Schmidt 2008) or metasomatised eclogite (Pyle and Haggerty 1994). Alternatively, the calcic carbonatite may form also by reaction of dolomitic melt with the depleted upper mantle and by partial melting of the carbonated upper mantle (Kogarko et al. 1995).

The C and O stable isotope ratios in the Hajnáčka carbonatite project along the devolatilization trend of carbonatites derived by partial melting of crustal material subducted beneath the Pannonian basin (Demény et al. 2004, 2010; Supplementary Fig. 2); this confirms the contamination of the basalt produced in the zone of partial melting by the carbonatite from the metasomatised mantle wedge above the subducted slab of oceanic crust. The basalt contamination provides an effective mechanism for overcoming the thermal barrier along the crust-mantle boundary, and for transfer of the subduction-related carbonatite into superimposed intra-continental rift magmatic assemblages.

Acknowledgements: Financial support was provided by VEGA grant 2/0069/13. Establishment of Raman and X-ray Laboratories was supported by the European Regional Development Fund under project of the Centre of Excellence for Integrated Research of the Earth's Geosphere (ITMS-26220120064). The constructive comments of Emma Humphreys-Williams, Anton Chakhmouradian, an anonymous referee, and Ian Swainson greatly improved the manuscript.

References

Bailey, D.K. (1993) Carbonate magmas. Journal of the Geological Society London, 150, 637-651.

Bali, E., Szabó, Cs., Vaselli, O., and Török, K. (2002) Significance of silicate melt pockets in upper mantle xenoliths from the Bakony-Balaton Highland Volcanic Field, Western Hungary. Lithos, 61, 79-102.

Bell, K. and Simonetti, A. (2010) Source of parental melts to carbonatites – critical isotopic constraints. Mineralogy and Petrology, 98, 77-89.

Brooker, R.A. and Kjarsgaard, B.A. (2011) Silicate-carbonate liquid immiscibility and phase relations in the system SiO_2-Na_2O-Al_2O_3-CaO-CO_2 at 0.1-2.5 GPa with applications to carbonatite genesis. Journal of Petrology, 52, 1281-1305.

Chacko, T., Mayeda, T.K., Clayton, R.N. and Goldsmith, J.R. (1991) Oxygen and carbon isotope fractionations between CO_2 and calcite. Geochimica et Cosmochimica Acta, 55, 2867-2882.

Chalot-Prat, F. and Arnold, M. (1999) Immiscibility between calciocarbonatitic and silicate melts and related wall rock reactions in the upper mantle: a natural case study from Romanian mantle xenoliths. Lithos, 46, 627-659.

Demény, A., Vennemann, T.W., Hegner, E., Nagy, G., Milton, J.A., Embey-Isztin, A., and Homonnay, Z. (2004) Trace element and C-O-Sr-Nd isotope evidence for subduction-related carbonate-silicate melts in mantle xenoliths (Pannonian Basin, Hungary). Lithos, 75, 89-113.

Demény, A., Dallai, L., Frezzotti, M.-L., Vennemann, T.W., Embey-Isztin, A., Dobosi, G., and Nagy, G. (2010) Origin of CO_2 and carbonate veins in mantle-derived xenoliths in the Pannonian Basin. Lithos, 117, 172-182.

Dérerová, J., Zeyen, H., Bielik, M., and Salman, K. (2006) Application of integrated geophysical modeling for determination of the continental lithospheric thermal structure in the eastern Carpathians. Tectonics, 25, TC3009.

Guzmicz, T., Kodolányi, J., Kovács, I., Szabó, Cs., Bali, E., and Ntaflos, T. (2008) Primary carbonatite melt inclusions in apatite and in K-feldspar of clinopyroxene-rich mantle xenoliths hosted in lamprophyre dikes (Hungary). Mineralogy and Petrology, 94, 225-242.

Hacker, B.R., Kirby, S.H., and Bohlen, S.R. (1992) Time and metamorphic petrology: Calcite to aragonite experiments. Science, 258, 110-112.

Harmer, R.E. (1999) The petrogenetic association of carbonatite and alkaline magmatism: constraints from the Spitskop complex, south Africa. Journal of Petrology, 40, 525-548.

Harmer, R.E. and Gittins, J. (1997) The origin of dolomitic carbonatites: field and experimental constraints. Journal of African Earth Sciences, 25, 5-28.

Humpreys, E.R., Bailey, K., Hawkesworth, Ch.J., Wall, F., Najorka, J., and Rankin, A.H. (2010) Aragonite in olivine from Calatrava, Spain – Evidence for mantle carbonatite melts from > 100 km depth. Geology, 38, 911-914.

Hurai, V., Huraiová, M., Konečný, P., and Thomas, R. (2007) Mineral-fluid-melt composition of carbonate-bearing cumulate xenoliths in Tertiary alkali basalts of southern Slovakia. Mineralogical Magazine 71, 17-33.

Keller, J. and Zaitsev, A.N. (2006) Calciocarbonatite dykes at Oldoinyo Lengai, Tanzania: The fate of natrocarbonatite. Canadian Mineralogist, 44, 857–876.

Kogarko, L.N., Henderson, C.M.B., and Pacheco, H. (1995) Primary Ca-rich carbonatite magma and carbonate-silicate-sulphide liquid immiscibility in the upper mantle. Contributions to Mineralogy and Petrology, 121, 267-274.

Konečný, V., Kováč, M., Lexa, J., and Šefara, J. (2002) Neogene evolution of the Carpatho-Pannonian region: an interplay of subduction and back-arc diapiric uprise in the mantle. EGU Stephan Mueller Special Publication Series, 1, 105-123.

Lee, W.-J. and Wyllie, P.J. (1998a) Process of crustal carbonatite formation by liquid immiscibility and differentiation, elucidated by model systems. Journal of Petrology, 39, 2005-2013.

Lee, W.-J. and Wyllie, P.J. (1998b) Petrogenesis of carbonatite magmas from mantle to crust, constrained by the system CaO-(MgO+FeO*)-(Na_2O+K_2O)-(SiO_2+Al_2O_3+TiO_2)-CO_2. Journal of Petrology, 39, 495-517.

Nemcok, M., Pospisil, L., Lexa, J., and Donelick, R.A. (1998) Tertiary subduction and slab break-off model of the Carpathian-Pannonian region. Tectonophysics, 295, 307-340.

Pyle, J.M. and Haggerty, S.E. (1994) Silicate-carbonate liquid immiscibility in upper-mantle eclogites: Implications for natrosilicic and carbonatitic conjugate melts. Geochimica et Cosmochimica Acta, 58, 2997-3011.

Sahagian, D.L. and Proussevitch, A.A. (1992) Bubbles in volcanic systems. Nature, 359, 485.

Tašárová, A., Afonso, J.C., Bielik, M., Götze, H.-J., and Hók, J. (2009) The lithospheric structure of the Western Carpathian-Pannonian Basin region based on the CELEBRATION 2000 seismic experiment and gravity modelling. Tectonophysics, 475, 454-469.

Thomsen, T.B. and Schmidt, M.W. (2008) Melting of carbonated pelites at 2.5-5.0 GPa, silicate-carbonatite liquid immiscibility, and potassium-carbon metasomatism of the mantle. Earth and Planetary Science Letters, 267, 17-31.

Vass, D., Elečko, M., and Konečný, V., Eds. (2007) Geology of Lučenská kotlina Depression and Cerová vrchovina Upland, 284 p. Štátny Geologický ústav D. Štúra, Bratislava, Slovakia.

Woolley, A.R. and Kjarsgaard, B.A. (2008) Paragenetic types of carbonatite as indicated by the diversity and relative abundances of associated silicate rocks: Evidence from a global database. Canadian Mineralogist, 46, 741-752.

Wyllie, P.J. and Boettcher, A.L. (1969) Liquidus phase relationships in the system CaO-CO_2-H_2O to 40 kilobars pressure with petrological applications. American Journal of Science, 267A, 489-508.

Figure Captions

Figure 1. a) Carbonated syenite xenolith in a basalt bomb embedded in welded tuff breccia. **b**) Back-scattered electron image of carbonated syenite xenolith (HA-8) showing calcitic matrix (Cal) with dispersed aragonite crystals (Arg) interstitial to potassium feldspar (Kfs) with inclusions of ilmenite (Ilm) and hercynite (Sp). Note aragonite crystals growing directly on corroded feldspar in the lower right part of the photomicrograph. **c**) Plane-polarized transmitted light image of carbonatite xenolith (HA-9) showing the contact between bladed aragonite crystals (Arg) and polygonal calcite matrix with a fibrous microtexture (Cal).

Figure 2. False-color X-ray maps of aragonite crystals within the calcitic matrix of carbonatite HA-9 (**a-c**), and carbonated syenite HA-8 (**d**). Preferential partitioning of Sr in the aragonite, competitive behavior of Mg and P in the calcite, and bending of the calcite fibers around the aragonite crystals reminiscent of a fluvial magmatic texture are observed.

Figure 3. False-color map of Raman intensities between 600 and 1200 cm^{-1} reveals growth zoning of aragonite, and the patchy domain texture of the associated calcitic matrix (see Figure 1c for comparison). Low-resolution (1.2 cm/pixel) spectra in the insets correspond to the places marked by arrows and open circles in the Raman maps.

Figure 4. Phase diagram of the CaO-H_2O-CO_2 system (Wyllie and Boettcher 1969) plotted onto geophysical boundaries and mantle geotherm of the northern Pannonian lithosphere (Dérerová et al. 2006), and stability field of carbonatite (diagonally striped area) mobilized from

277 subducted oceanic crust (Thomsen and Schmidt 2008). Abbreviations: Arg – aragonite, Cal –
278 calcite.

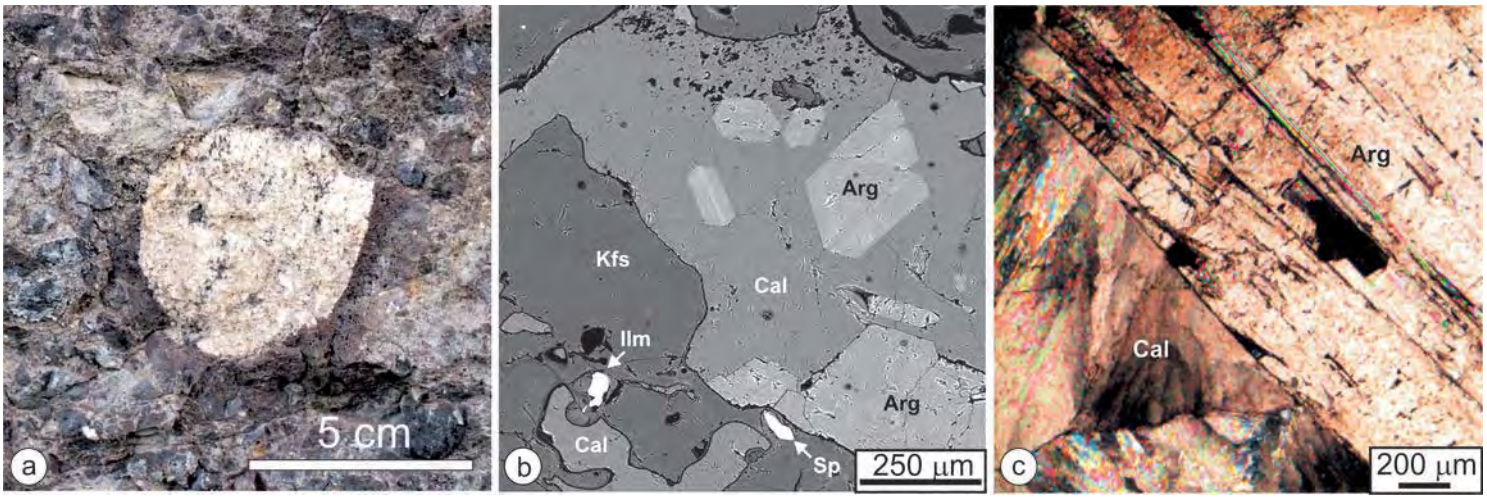
a
5 cm
b
Arg
Kfs
Cal
Ilm
Arg
Cal
Sp
250 μm
c
Arg
Cal
200 μm

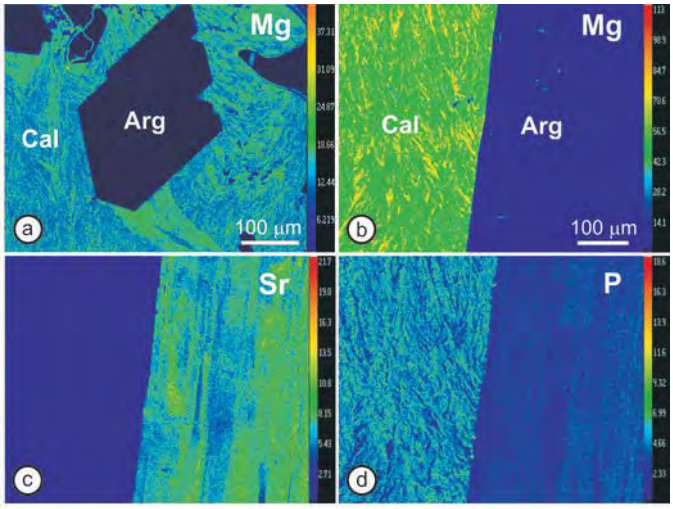
Mg
Arg
Cal
100 µm
a
Mg
Cal
Arg
100 µm
b
Sr
c
P
d

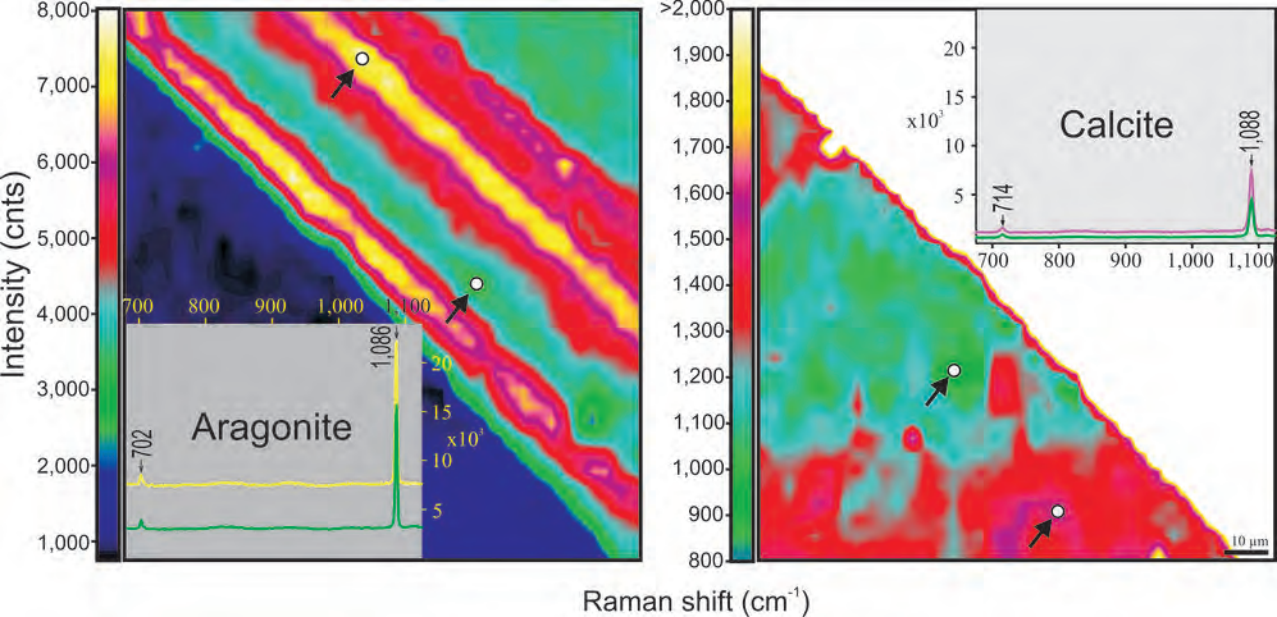
Intensity (cnts)
8,000
7,000
6,000
5,000
4,000
3,000
2,000
1,000
Aragonite
1,086
702
700
800
900
1,000
1,100
20
15
10
5
x10³
>2,000
1,900
1,800
1,700
1,600
1,500
1,400
1,300
1,200
1,100
1,000
900
800
Calcite
1,088
714
10 µm
Raman shift (cm⁻¹)

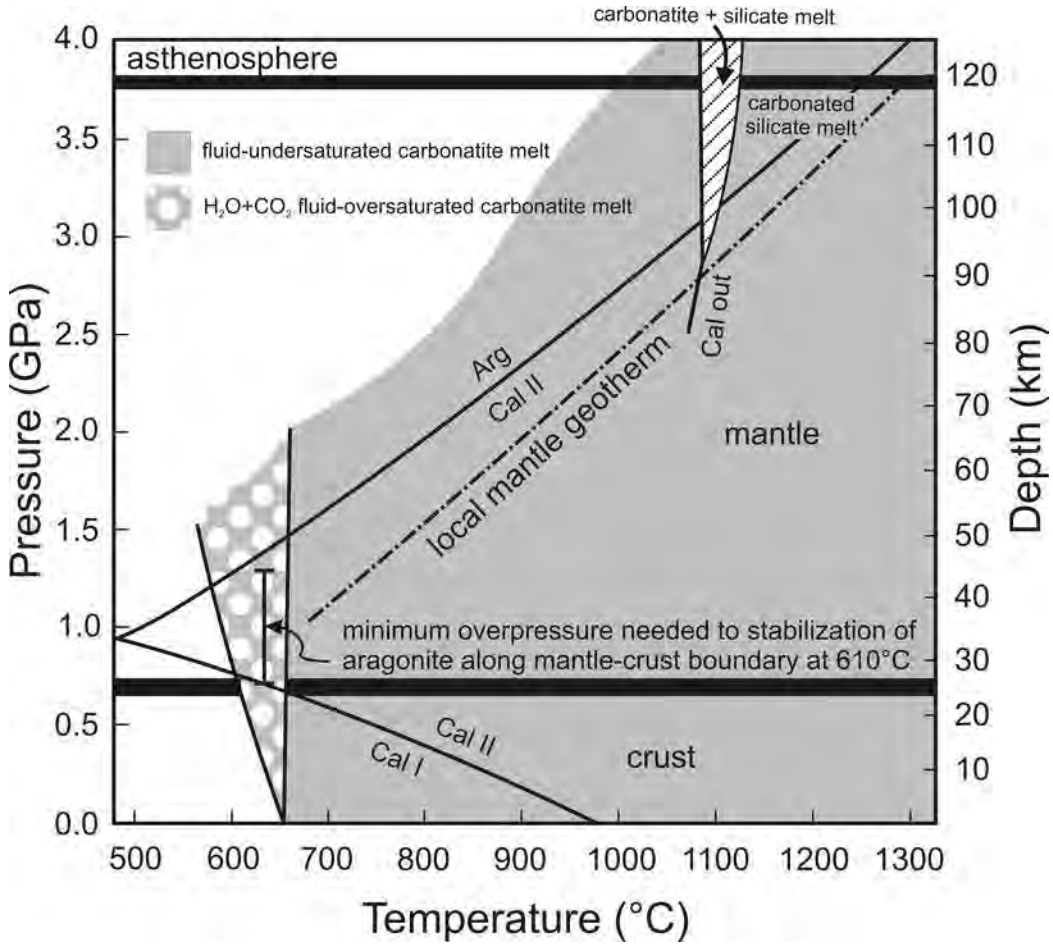
carbonatite + silicate melt
asthenosphere
carbonated
silicate melt
fluid-undersaturated carbonatite melt
H2O+CO2 fluid-oversaturated carbonatite melt
Arg
Cal II
Cal out
local mantle geotherm
mantle
minimum overpressure needed to stabilization of
aragonite along mantle-crust boundary at 610°C
Cal II
Cal I
crust
Pressure (GPa)
Depth (km)
Temperature (°C)
4.0
3.5
3.0
2.5
2.0
1.5
1.0
0.5
0.0
120
110
100
90
80
70
60
50
40
30
20
10
500
600
700
800
900
1000
1100
1200
1300